STAR FORMATION NEWSLETTER #298 6 - 10

泉奈都子

A study of dust properties in the inner sub-au region of the Herbig Ae star HD 169142 with VLTI/PIONIER

L. Chen et al. Accepted by A&A http://arxiv.org/pdf/1709.06514

HD 169142 のdiskに対する近赤外の観測

- **HD 169412**
  - group I のSED (MIRかFIRにcold component有)を持つHerbig Ae star
  - Diskの内部にgapが存在している
    - inner: ~ 20au, outer: ~ 40-70au, ~85au
  - Dustとgasの分布が異なる
  - 10年間でNIRのexcessが45%減少している
    （pre-2000 high state => post-2000 low state）
    - 内側にある optically thin の dustの分布の変動が原因と考えられる

- **観測**
  - VLTI/PIONIER
  - 2011年に一晩、2013年に3晩

- **モデル**
  - Geometric modeling
  - Monte-Carlo radiative transfer modeling

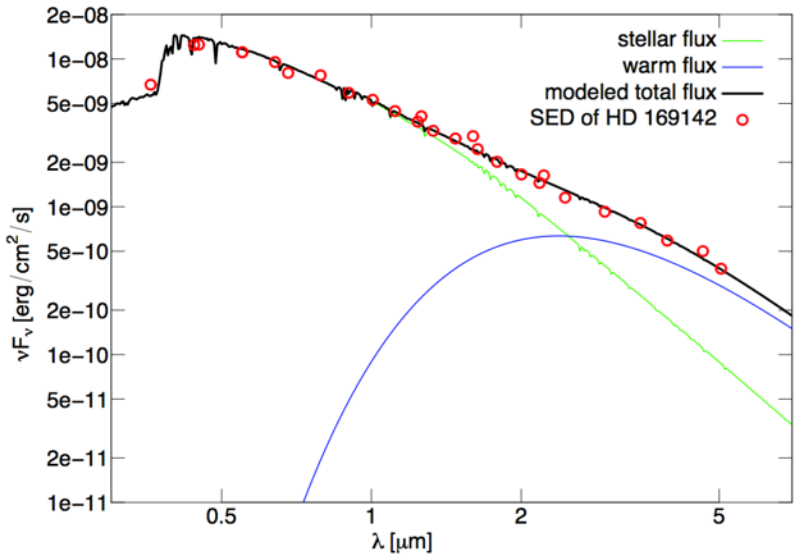

Fig. 3. SED of HD 169142, and our Kurucz plus blackbody fitting.

● 結果

- NIRを放射するhot dustが ~ 0.07 auのところに存在 (T ~ 1500 K)
  - 1.0 μm 以上のoptically thinなdustの存在 or Optically thickなcomponentの存在
  - Smallなoptically thinなdustはoverheatされるため、考えられない
- pre-2000 high state => post-2000 low state の進化のシナリオ
  - 1. inner dustはoptically thin => その大部分が失われる
  - 2. inner dustはoptically thin componentと optically thick core
    => optically thin componentのみ失われる

a

Parameter	Parameter range	Steps	Model AF1
L_* [$L_\odot$]	[4, 5]	5	4.8
i [°]	0	–	0
PA [°]	0	–	0
Component 1 (inner disk)			
R_{in} [au]	[0.04, 0.2]	12	0.072
W_{ring}	0.5	–	0.5
h_{in}	0.6	–	0.6
q	0	–	0
p	0	–	0
τ	[0.05, 0.2]	12	0.083
n	[−3.5, −2]	4	−2
f_{carbon}	0.5	–	0.5
Component 2 (halo)			
k	0.13	–	0.13
χ^2_{red}			1.36

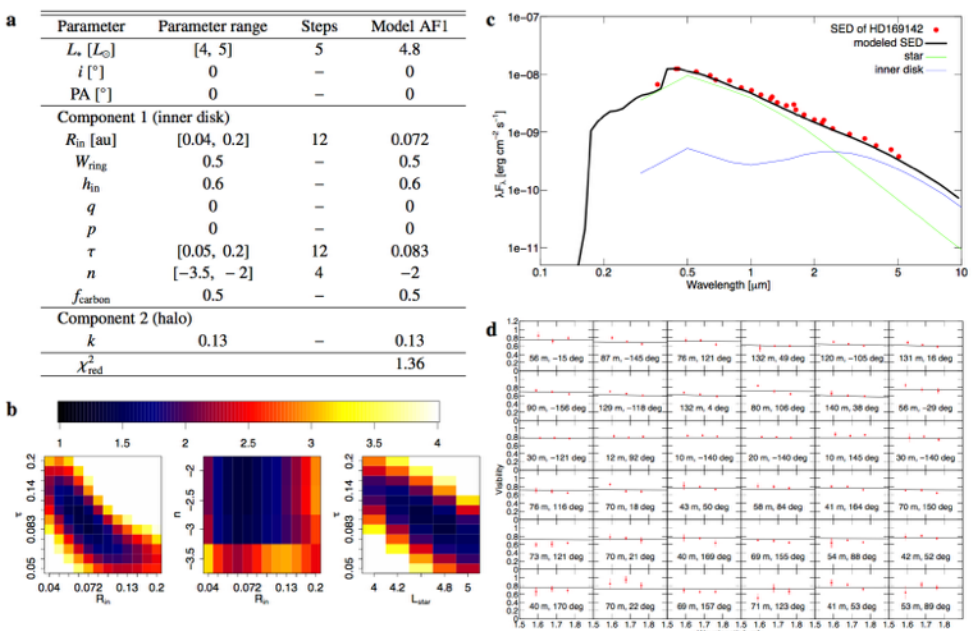

Fig. 4. Model scanning run AF (optically thin inner disk), and the model parameters of the best model AF1 with minimum χ^2_{red}, which is calculated by comparing each model with the data set.
a: Parameter ranges of model scanning run AF, number of tested parameter values (steps) per parameter, and parameters of the best model AF1. The listed parameters are:
L_* = stellar luminosity ,
i = inclination of the disk,
PA = positional angle of rotation axis the disk,
and the following parameters for the inner sub-AU disk,
R_{in} = inner radius of the inner disk ,
$W_{ring} = (R_{out} - R_{in})/R_{in}$ (relative radial width of the inner component),
R_{out} = outer radius of the inner disk ,
h_{in} = scale height of the inner disk at its inner radius,
q = scale-height power-law index of the inner disk,
p = surface-density power-law index,
τ = Planck-averaged midplane optical depth at 7500 K,
n = power-law index of grain size distribution,
f_{carbon} = fraction of carbon in the dust.

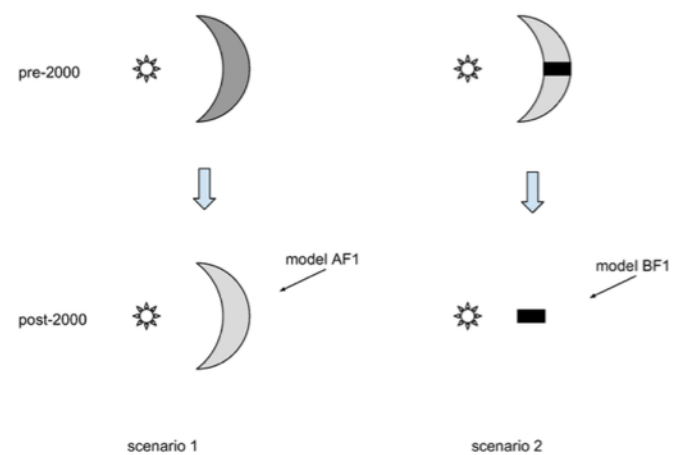

Fig. 6. Sketch of the scenarios for the evolution of the inner sub-AU region in HD 169142.

GMC Collisions As Triggers of Star Formation. IV. The Role of Ambipolar Diffusion

Duncan. Christie et al. Accepted by ApJ https://arxiv.org/pdf/1706.07032

GMC同士のcollisionの際のambipolar diffusionによる影響を調べる

- モデル
  - Enzo magnetohydrodynamics code (include ambipolar diffusion)

Table 1. Momentum Exchange Coefficients

Interaction	$\langle\sigma w\rangle_{\rm in}$ $(\times 10^{-9}$ cm^3 s$^{-1})$	Source	Comment
Collisions with e^-			
e^--H	$\sqrt{T}\,(2.841+0.093\theta+0.245\theta^2-0.089\theta^3)$	Pinto & Galli (2008)	
e^--He	$0.428\sqrt{T}$	Pinto & Galli (2008)	
e^--H_2	$\sqrt{T}\,(0.535+0.203\theta-0.163\theta^2+0.050\theta^3)$	Pinto & Galli (2008)	
Collisions with H^+			
H^+-H	$0.649T^{0.375}$	Pinto & Galli (2008)	
H^+-He	$1.424+7.438\times10^{-6}T-6.734\times10^{-9}T^2$	Pinto & Galli (2008)	
H^+-H_2	$1.003+0.050\theta+0.136\theta^2-0.014\theta^3$	Pinto & Galli (2008)	
Collisions with He^+			
He^+-H	4.71×10^{-1}	Schunk & Nagy (2004)	
He^+-He	$2.0\times8.73\times10^{-2}(1-0.093\log T)^2$	Schunk & Nagy (2004)	
Collisions with H_3^+			
H_3^+-H_2	$2.693-1.238\theta+0.663\theta^2-0.089\theta^3$	Pinto & Galli (2008)	
Collisions with molecular ions M^+ *other than* H_3^+			
M^+-H_2	$\sqrt{T}\,(1.476-1.409\theta+0.555\theta^2-0.0775\theta^3)$	Pinto & Galli (2008)	Adopted rate for HCO^+
Collisions with atomic ions A^+ *other than* H^+, He^+			
A^+-H	$1.983+0.425\theta-0.431\theta^2+0.114\theta^3$	Pinto & Galli (2008)	Adopted rate for C^+

NOTE—The momentum exchange coefficients are functions of both T and $\theta=\log(T/K)$.

Table 2. Summary of Simulations

Model	Name	$v_{\rm rel}$ (km s^{-1})	B (μG)	AD
Fiducial B-Field Strength				
1	Ideal Colliding	10	10	No
2	Ideal Non-colliding	0	10	No
3	AD Colliding	10	10	Yes
4	AD Non-colliding	0	10	Yes
Strong B-Field				
5	Ideal Colliding	10	30	No
6	Ideal Non-colliding	0	30	No
7	AD Colliding	10	30	Yes
8	AD Non-colliding	0	30	Yes

● 結果

- Ambipolar diffusion は B-fieldが強い時（30 μG）に、collisionに対する影響が最も強くなる
- Core ($n_H \geqq 10^6$ cm^{-3}) の生成効率はAmbipolar diffusionを入れた方が一桁高くなる（0.2 % => 2 %）

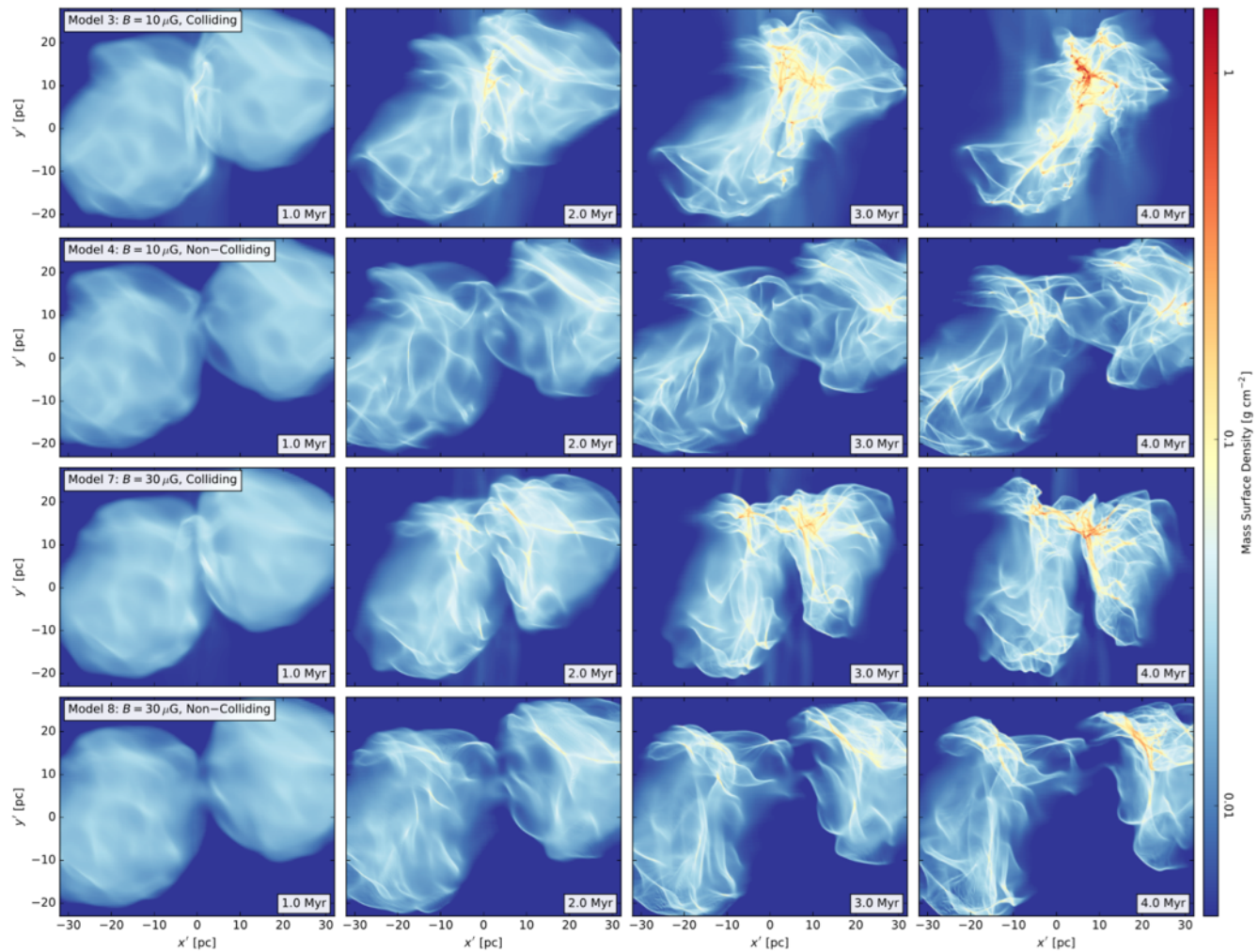

Figure 3. Evolution of mass surface density from 1 to 4 Myr (panels left to right) for each AD run. First row: $B = 10\,\mu$G, colliding; 2nd row: $B = 10\,\mu$G, non-colliding; 3rd row: $B = 30\,\mu$G, colliding; bottom row: $B = 30\,\mu$G, non-colliding. These figures show the overall evolution of cloud structures as a result of internal turbulence and, in the first and third rows, of the 10 km s^{-1} GMC-GMC collision. Density differences resulting from AD compared to the ideal MHD case occurring on small scales are presented in the next figures.

ALMA shows that gas reservoirs of star-forming disks over the past 3 billion years are not predominantly molecular

Luca Cortese et al. Accepted by ApJL http://arxiv.org/pdf/1709.07933

Massive star-forming galaxy におけるCold hydrogen gasの中の原子、分子の割合

- **観測**
  - ターゲット: 5つの銀河（z= 0.2）
    <= HIGHz survey の一環
  - 望遠鏡：ALMA (^{12}CO(1-0)),
    Arecibo (HI),
    Keck (Hα spectroscopy)

Table 1. The cold gas content of HIGHz galaxies

AGC[a]	SDSS ID	z_{SDSS}	log(M_*)	S_{CO}	log(M_{H_2})	log(M_{H_2}/M_{HI})	log(SFR)
			$M_\odot$	Jy km s^{-1}	$M_\odot$		$M_\odot$ yr^{-1}
191728	J091957.00+013851.6	0.1763	10.89	2.91	10.15	−0.20	1.17
242091	J140522.72+052814.6	0.1954	11.03	1.55	9.97	−0.61	1.24
242147	J142735.69+033434.2	0.2455	11.26	2.32	10.35	−0.46	1.43
249559	J144518.88+025012.3	0.1906	11.17	3.86	10.34	−0.06	1.19
252580	J151337.28+041921.1	0.1754	10.78	0.74	9.55	−1.04	0.79

[a] Arecibo General Catalog, maintained by M. P. Haynes and R. Giovanelli at Cornell University

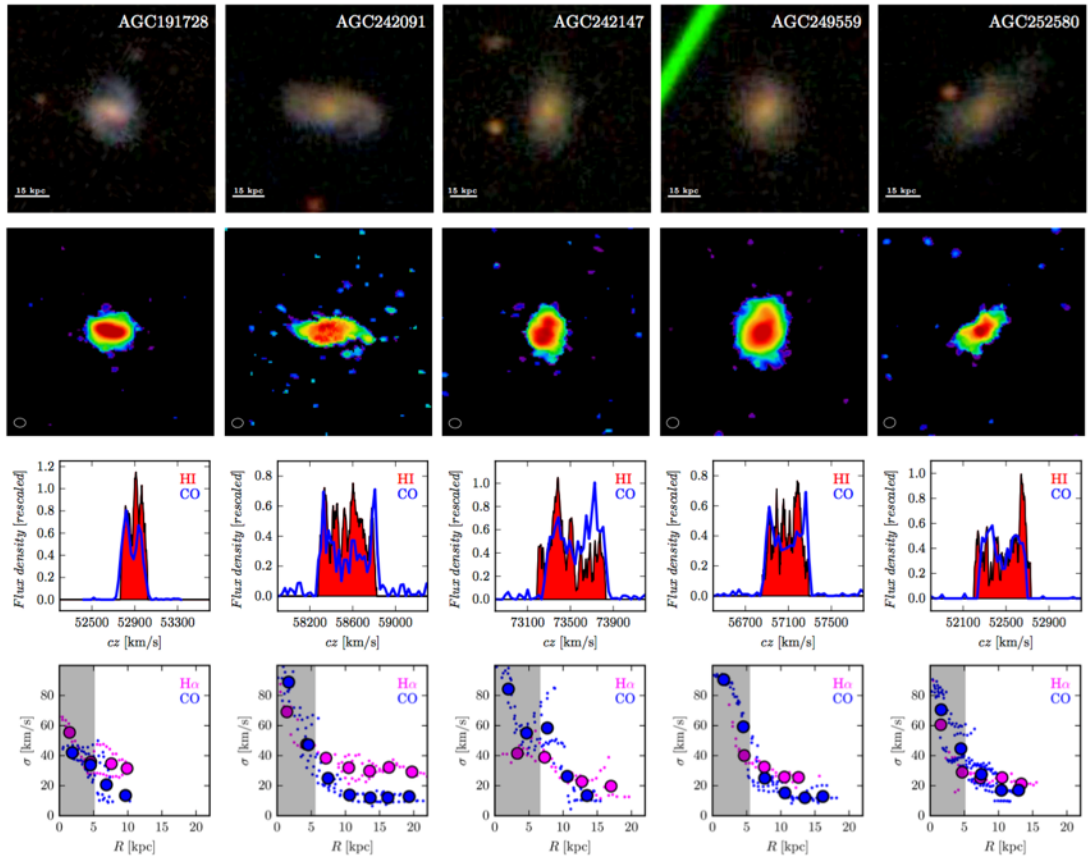

Figure 1. Multiwavelength properties of HIGHz galaxies. *Top rows*: Optical Sloan Digital Sky Survey color images and ALMA ^{12}CO(1-0) moment 0 maps. Both sets of images are 30″wide. The size of the synthesized ALMA beam is shown by the ellipse on the bottom left corner of the ^{12}CO(1-0) maps. *Third row:* comparison between the integrated Arecibo HI (red) and ALMA ^{12}CO(1-0) (blue) spectra. Flux densities have been scaled to facilitate the comparison. *Bottom row:* Hα (magenta) and ^{12}CO(1-0) (blue) velocity dispersion as a function of radius. Small points indicate individual measurements, whereas big circles show the averages estimated within 3 kpc wide bins. Averages are presented only when at least four measurements are available. The shaded region corresponds to one FWHM of the ALMA synthesized beam, where measurements are heavily affected by beam smearing.

● **結果**

- 今回観測した銀河（z ~ 0.2）のatomic-molecular hydrogenの割合 は近傍にある main sequence diskと変わらない
  => 少なくとも今より30億年前からは atomic gasが cold hydrogen gasの中で支配的である

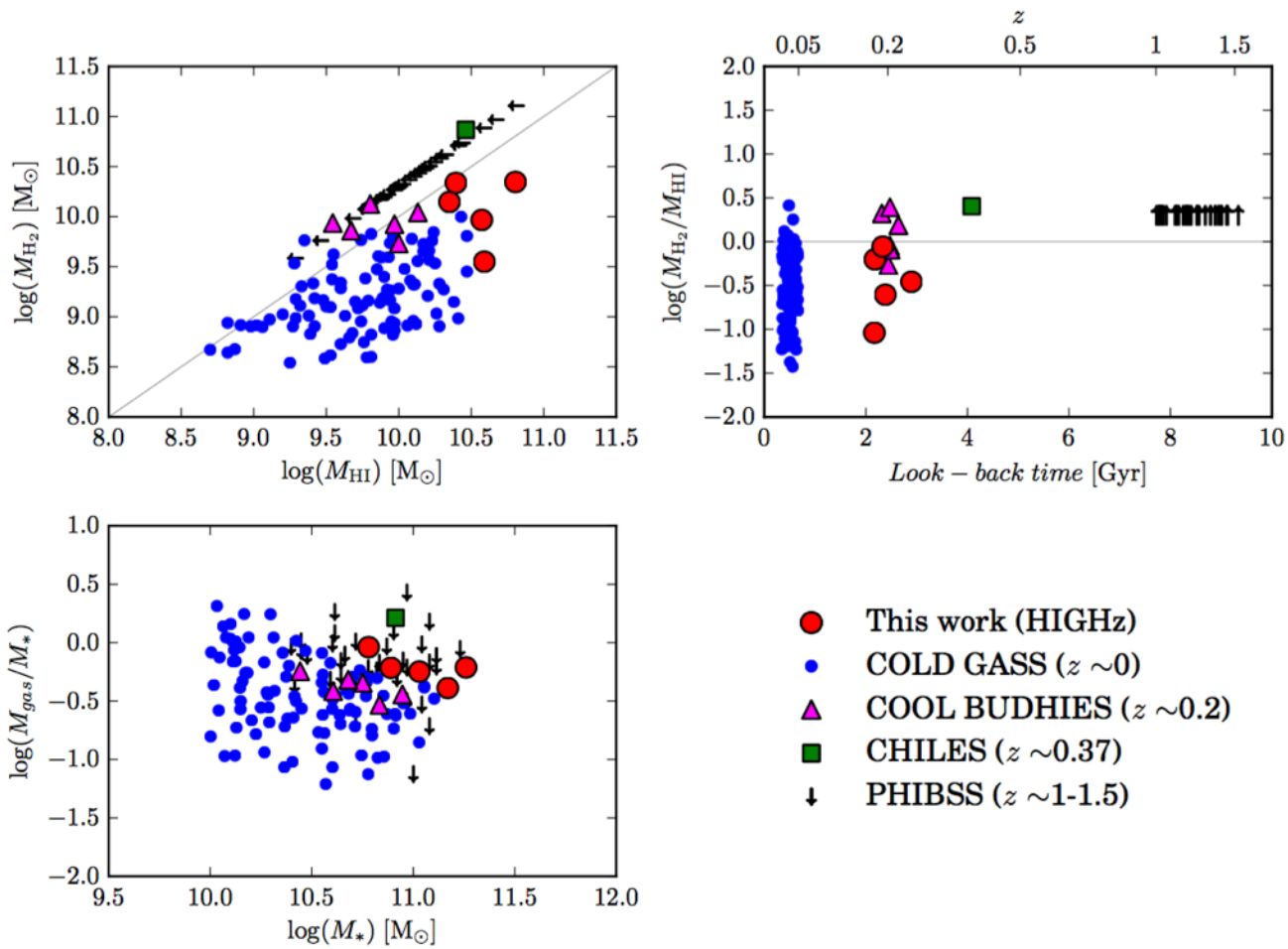

Figure 2. Cold gas reservoir of galaxies between $z \sim 0$ and ~ 1.5. The H_2 mass as a function of HI mass (top left), the evolution of the molecular-to-atomic mass ratio with redshift (top right) and the total cold gas fraction as a function of stellar mass (bottom right) are shown. Filled symbols indicate samples with measurements of both atomic and molecular hydrogen. The gray lines in the top panels show the boundary between the HI- (bottom) and H_2-dominated (top) regimes. Above $z \sim 0.4$, detecting HI in emission is unfeasible with current instruments; thus, PHIBSS galaxies are plotted as lower limits assuming $M_{H_2}/M_{HI} \geq 2$.

Interpretation of a Variable Reflection Nebula Associated with HBC 340 and HBC 341 NGC1333

S.E. Dam & L.A. Hillenbrand Accepted by AJ http://arxiv.org/pdf/1709.01503

NGC1333における変光の原因を探る

- **NGC1333**
  - おうぎ形をした変光星雲
  - HBC340 (K7e), HBC341 (M5e) に付随

- **観測**
  - R band, 長期: Palomar Transient Factory
  - B,V,R_C,I_C band, 1回: UH 2.2m
  - 600 nm, 800nm : HST (Survey data)
  - High-resolution optical spectra of HBC340 and HBC341 : Keck
  - Moderate-resolution NIR spectra (0.8 - 2.5 μm) : IRTF

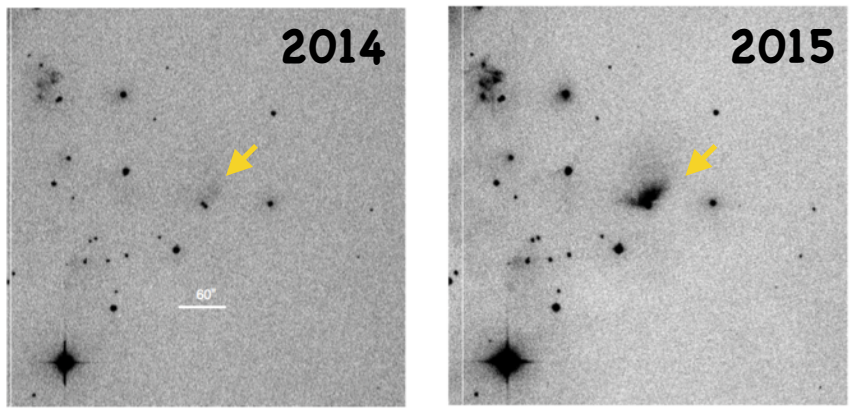

FIG. 1.— Palomar Transient Factory 500×500 arcsec, R−band images (north is up, east is to the left) of HBC 340 and its associated reflection nebula obtained near minimum light in September 2014 (left) and after recovering its former brightness level in January 2015 (right). To the northeast lies the complex series of knots of emission that comprise Herbig-Haro (HH) 12, one of the more prominent HH objects in the NGC 1333 star forming region.

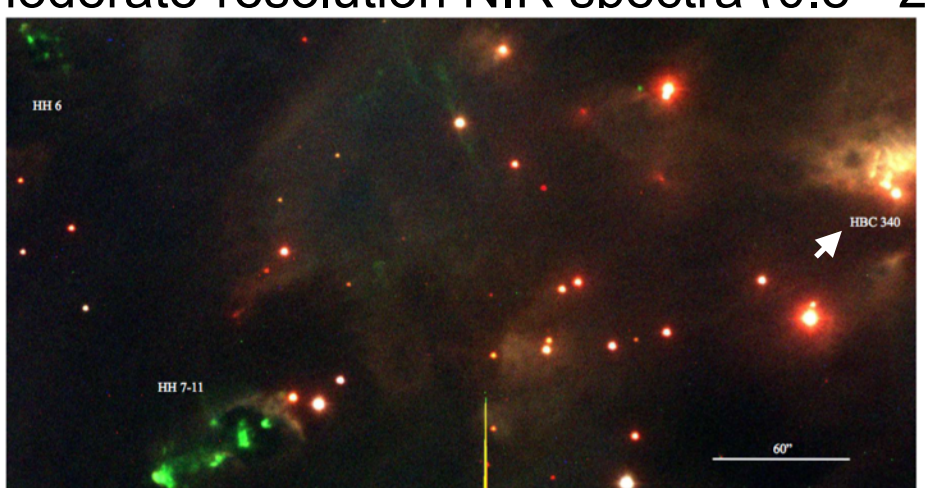

FIG. 3.— Composite, three-color VR_CI_C image of the HBC 340 region in NGC 1333 obtained using the Tek2K CCD camera on the UH 2.2 m telescope in October 1999 oriented such that north is up, east is to the left. The field presented here spans several arcminutes from HBC 340 and the variable reflection nebula near the right edge, to the impressive series of HH objects 7-11 on the bottom left. HH 6 lies near the top, left edge of the frame. The image suggests that extensive molecular material lies in the foreground of HBC 340 and HBC 341, but that an opening to the north reveals the illuminated interior of the evacuated cavity.

● 結果

- HBC340, 341はともに強いHα線、禁制線を放射 => accretion, outflowとconsistent
- NGC1333における変光はHBC340の変光によるもの
- protostarにおける短期間の変動は何かイレギュラーなaccretionによるもの（Balmer, Paschen, Brachtet emission, NIR excess）
- protostarにおける数100日間スケールでの変動はcircumstellar material (HBC340Ab)の軌道によるもの
- HSTの観測結果により、HBC340の伴星 (HBC340B)を発見
- 2014年の後期からHBC340の明るさが減らないのは EXor-likeのoutburstによるもの

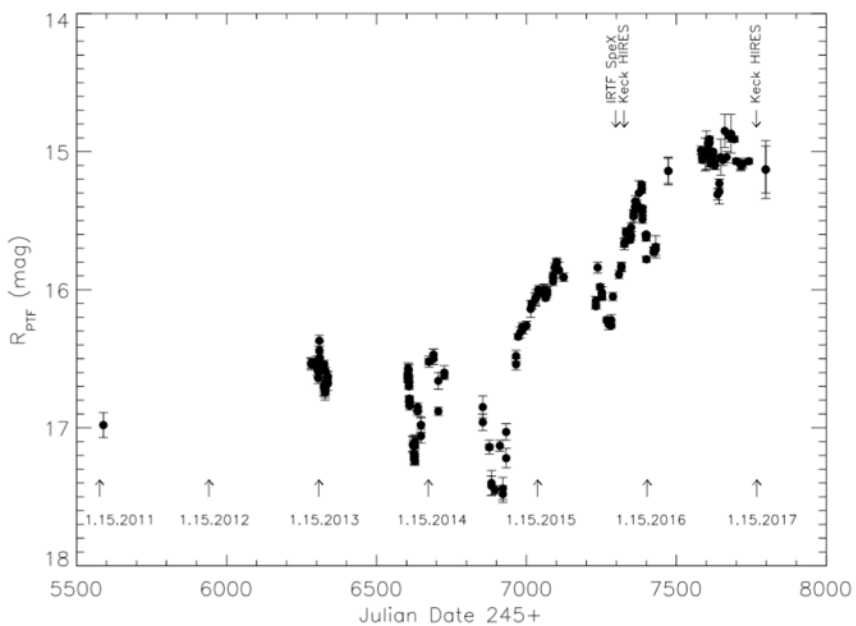

FIG. 6.— The PTF R−band light curve of HBC 340 plotted as a function of Julian date. The figure spans over six years of low-cadence observations made of the region. HBC 340 has brightened by more than two magnitudes since a deep minimum that occurred in late August and early September 2014. Several local minima are evident in the light curve, which correspond to faint states of the diffuse nebula.

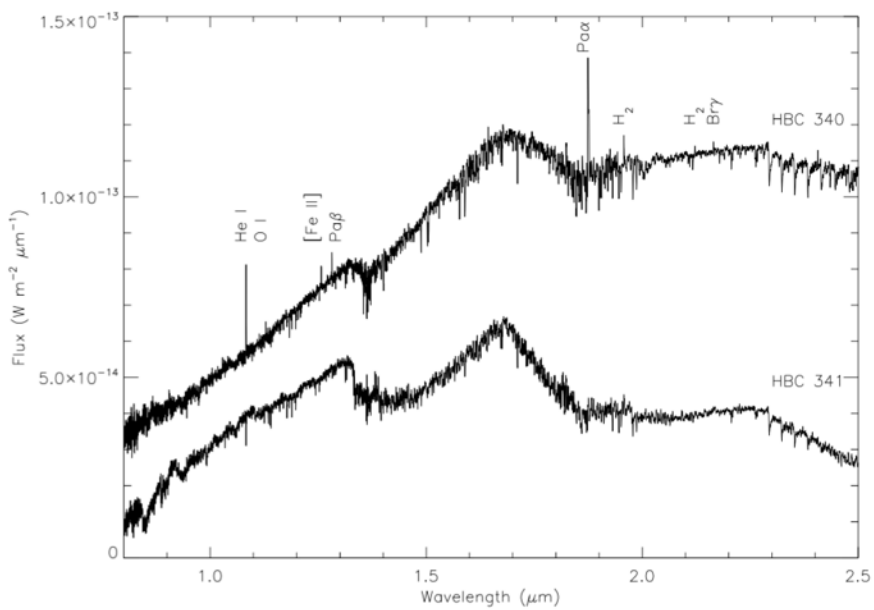

FIG. 9.— Telluric corrected, merged order SpeX spectra of HBC 340 and HBC 341. The spectrum of HBC 340 is offset by 2×10^{-14} W m^{-2} μm^{-1} to separate it from the spectrum of HBC 341 at blue wavelengths. Emission features characteristic of circumstellar disk accretion (He I λ10830, Paβ, Brγ) are present in the spectrum of HBC 340, but not in that of HBC 341. The slopes of both SEDs beyond two microns, however, are suggestive of excess infrared emission, indicative of circumstellar disks.

IN-SYNC. V. Stellar Kinematics and Dynamics in the Orion A Molecular Cloud

Nicola Da Rio et al. Accepted by ApJ https://arxiv.org/pdf/1702.04113

Orion A Star-forming region 内部の星のkinematics

- **Data**
  - IN-SYNC (INfrared Spectra of Young Nebulous Clusters) survey のデータ
    - Velocity precisions ~ 0.3 km/s
    - Orion A star-forming regionの内部のyoung clusterから ~ 2700個もの星のspectraを取得
    - radial velocity を用いてstellar kinematics を調べる

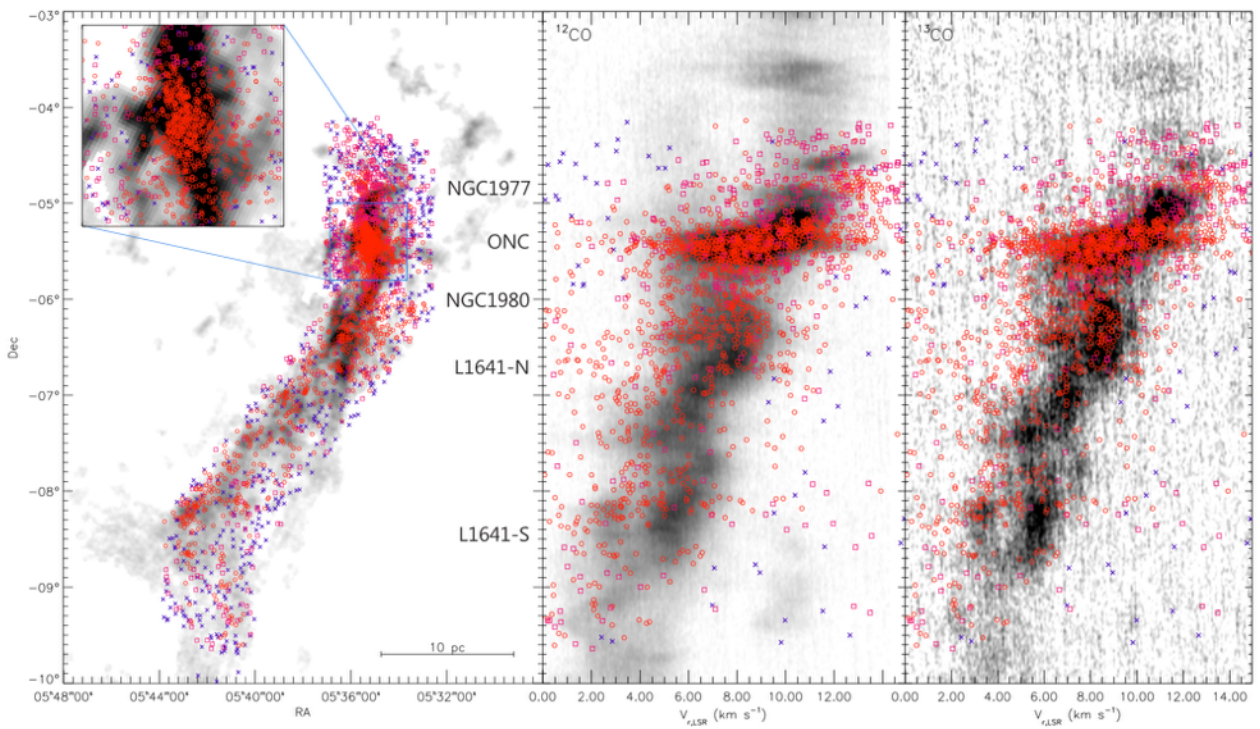

FIG. 1.— *Left panel:* spatial distribution of the IN-SYNC targets, overplotted on a ^{13}CO(2-1) map from Nishimura et al. (2015). Red circles indicate known members from the literature, magenta squares new candidate members from Paper IV, blue crosses remaining sources, likely non-members. *Middle and right panels*: position-velocity diagram for the targets, compared to either ^{12}CO(2-1) or ^{13}CO(2-1) data.

- **結果**
  - 全体的には若い星の平均のradial velocityと周囲のgasのradial velocityは似ている
  - Spatial, kinematic substructuresの存在を確認
    - ほとんどはcloudのlow-density regionに存在
    - ONCでは見られない <= ONCのclusterの方がより進化している

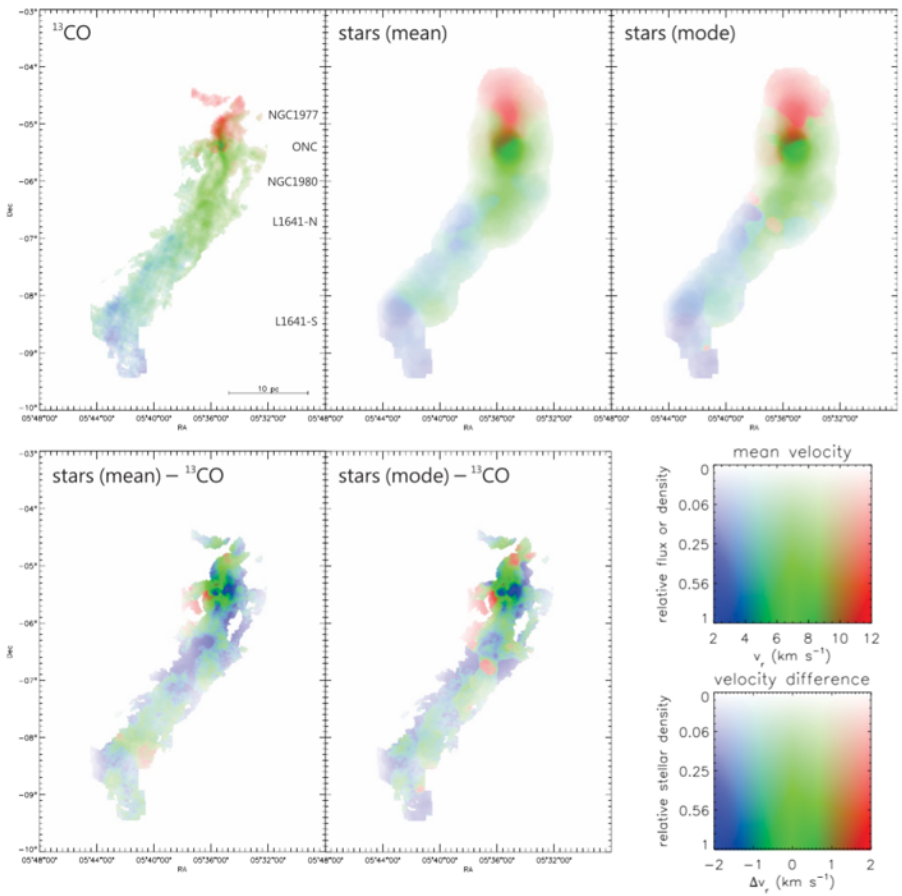

FIG. 3.— Maps of mean or mode velocity for gas and stars, and difference between stars and gas, color-coded as indicated in the legend.

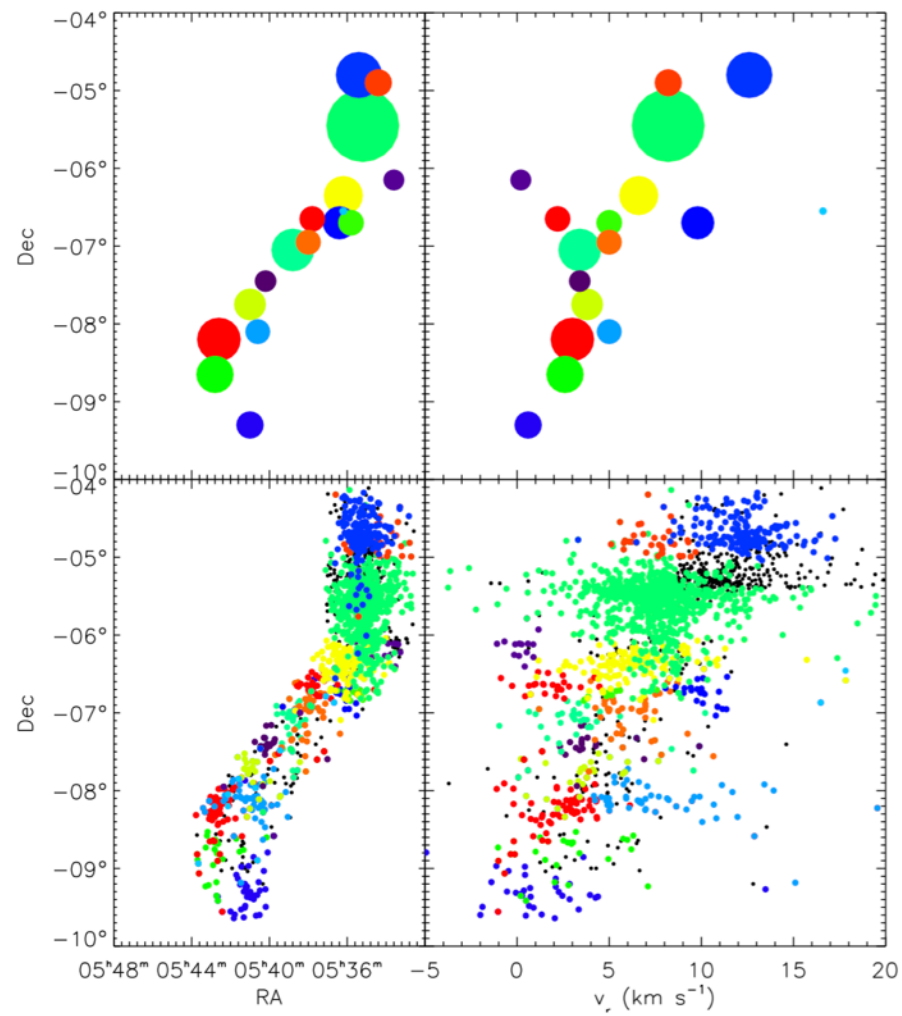

FIG. 6.— *Top panels:* position-position and position-velocity diagrams of the identified overdensities in *ppv* space. The size of the circles indicates the the local density of the structure in *ppv*, while the colors are arbitrarily chosen to easily distinguish between different groups. *Bottom panels:* position of the members in the same projection of the *ppv* space. Colored dots indicate stars associated in *ppv* to each of the identified substructures (see text), with colors corresponding to each structure in the upper panels.

● 結果

- Velocity dispersion（σ_v）はfilamentに沿って変動

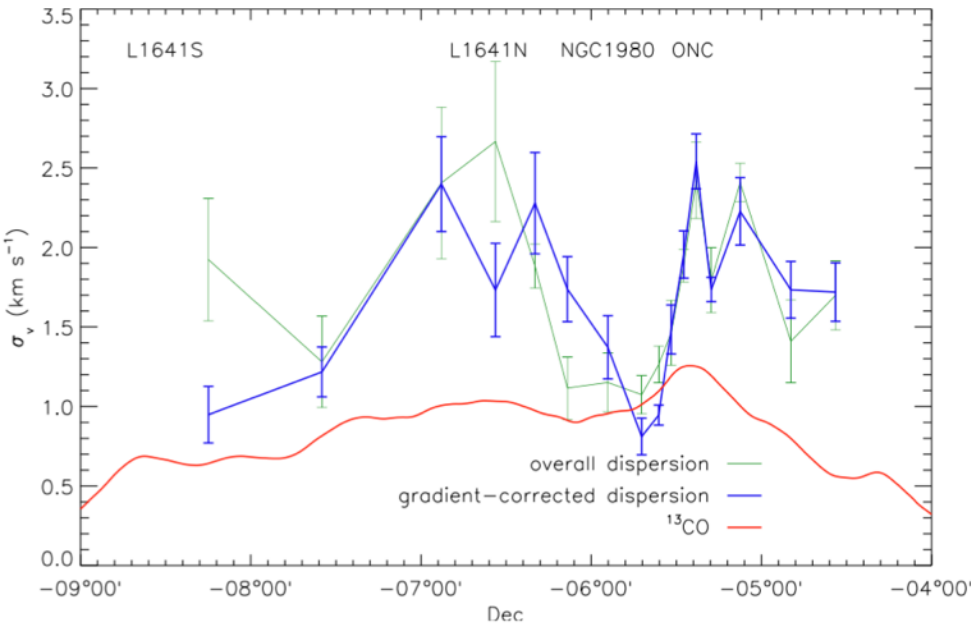

FIG. 11.— The velocity dispersion σ_v as a function of declina tion. The blue solid line represents the overall dispersion, correcte for measurement errors and binarity, in each declination bin. Th dashed blue line is the same with an additional correction for spa tial gradients in v_r in each sample (see text). The red solid line i the velocity dispersion of the gas from the survey of Nishimura e al. (2015).

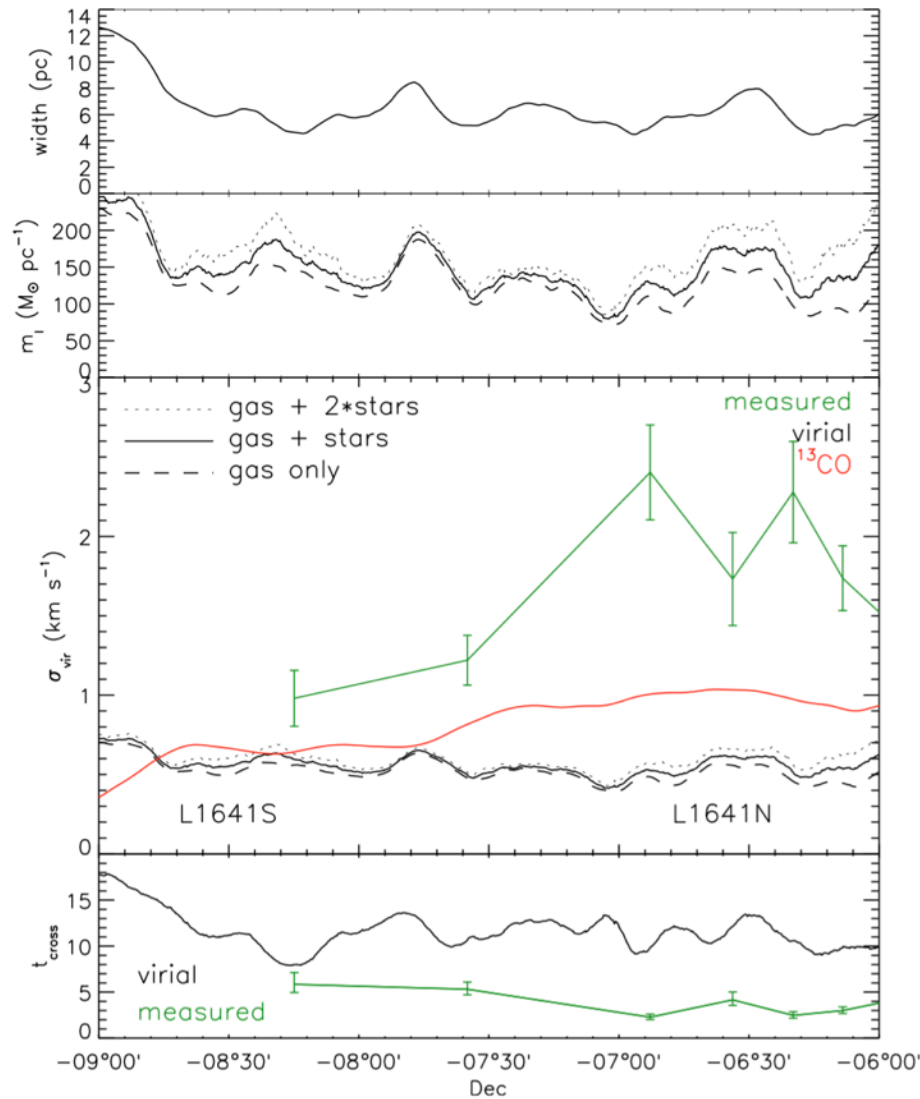

FIG. 13.— From top to bottom, as a function of declination: a) width of the filament, defined where $A_V \geq 0.3\ A_V$; b) mass per unit of length m_l; c) virial velocity dispersion σ_{vir} from Equation 1, compared with the observed dispersions for gas and stars; d) crossing time expected for σ_{vir} compared to the measured σ_v.